JOURNAL OF MATERIALS SCIENCE **34** (1999) 1107–1116

Low velocity response of a complex geometry pultruded glass/polyester composite

M. WISHEART, M. O. W. RICHARDSON*
Institute of Polymer Technology and Materials Engineering, Loughborough University, Loughborough, Leicestershire LE11 3TU, UK
E-mail: M.O.Richardson@lboro.ac.uk

This paper describes an investigation into the low velocity impact response on complex geometry sections taken from a pultruded glass/polyester product. The empirical impact behaviour of the system was evaluated using instrumented falling weight impact testing (IFWI) in conjunction with ultrasonic C-Scan, optical microscopy and thermal deply techniques to detect delamination, matrix cracking, and fibre breakage. © *1999 Kluwer Academic Publishers*

1. Introduction

Impact damage and the strength reductions which results even from low levels of damage is a major concern in fibre reinforced composite materials. Understanding complex and varied impact damage modes, including matrix cracking, delamination and fibre breakage, and interactions between the three, remains an area of high research interest [1, 2]. To this end much work has been performed on relatively simple plate coupons and indeed the impact response of simple coupons taken from the glass/polyester pultruded section which is the focus of this work, has been performed by the authors and is reported in detail elsewhere [3, 4] as is an investigation into strain-rate effects [5]. However the research described here concentrates on the impact behaviour of more complex geometry specimens.

The product's cross-section was double-skinned with longitudinal webs which represents quite a complex geometry. In general little work on impacts on complex structures has been published, but the webs act as stiffeners and some work on impacts on stiffened panels has been performed. Dorey [6] reported that the energy to cause BVID dropped significantly near the stiffeners, where the structure was less compliant and that the stiffeners caused damage to spread asymmetrically, as would be expected over an area of non-uniform stiffness. Davies and co-authors [7, 8] stated that impact forces will be higher in the stiffened regions, but that reduced deflections may lead to smaller strains and therefore less strain induced failure. At the edge of the stiffeners delaminations were formed, whilst impacts directly over the stiffener caused debonding between plate and stiffener. The damage tended to extend down the stiffener which would have a serious effect for a compression loaded panel. "Cratering" also occurred due to the very high forces induced in the stiffened regions. Cheung *et al*. [9] performed impacts on thin flat and blade stiffened carbon/epoxy panels. Tests were performed between, near, and directly over a stiffener and the extent of damage recorded. They concluded that the damage incurred depended on the impact location and that whilst flat panel damage remained local to the impact location, damage remote to the impact site was observed when the impacts were over a stiffener due to high stress concentrations at the skin-stiffener interface. Further work has been performed by Tabiei *et al*. [10, 11] who investigated the impact behaviour of pultruded box-beams for roadside safety structures. Due to fear of stiffener-panel debond, many manufacturers are using mechanical joining techniques to avoid this problem, indicating the level of concern associated with this problem.

2. Methodology

2.1. Impact testing

The tests were performed using the Instrumented Falling Weight Impact (IFWI) technique by employing a precision Impact Test Machine IFW 5 with a variable mass and geometry impactor. The impactor mass (10.8 kg) was kept constant throughout the tests and the impact energy altered by varying the impactor velocity (by altering the drop height) from very low energy up to final failure. The impactor had a 10 mm diameter hemi-spherical impactor tip and at each energy approximately five test were performed. A second-strike prevention system was employed, therefore it was possible to perform a detailed damage analysis on all the impacted specimens.

2.2. Damage analysis

Optical microscopy inspection was performed on sections cut from the damaged area to provided quantitative and qualitative information on matrix cracking and delamination patterns. In order to obtain a three-dimensional map of matrix cracking and delamination, the impacted specimens were cut into transverse strips

* Author to whom all correspondence should be addressed.

(a similar approach is described by Hong and Liu [12]). The specimens were cut, polished with progressively finer grades of silicon carbide, and then a highlighter pen drawn across the polished surface and the excess ink removed by wiping with a clean cloth. The remaining ink highlighted the matrix cracks and delaminations. Specimen was subjected to an **ultrasonic C-scan,** obtained via a 2.25 MHz alpha type transmitter employed with a Wells Krautkramer Flaw Detector USIP 12 system. The specimens chosen for **thermal deply analysis** were placed in a Eurotherm Muffle Furnace, situated in a standard fume cupboard, to burn off the resin. The technique was employed to obtain the extent of fibre breakage in the impacted specimen.

2.3. Specimen geometry

The sections tested were taken from the pultruded composite section as shown in Fig. 1. The primary material components of the section were E-glass fibres and isophthalic polyester resin. The outer skins consist of unidirectional fibres (UD) sandwiched between continuous filament mats (CFM).

The geometry of the test sections are shown in Figs 2 and 3 and consisted of either three- or five-box sections cut from the pultrusion. The three-box section was 200 mm wide by 255 m long, whilst the five-box section was 200 mm by 425 mm. Both were simply supported on 16 mm diameter rollers midway between the webs of the end boxes. Three separate series of tests were performed on each section by altering the position of the impactor strike as described below, along the same principles as Phan and Kesack [13] and Cheung *et al.* [9] in their work on residual strength and damage growth of impacted stiffened composite panels respectively. For the "central" impact site tests, the impactor struck the box section precisely mid-way between the webs of the central box, which was therefore halfway between the supports, and is shown as impactor position (a) in Figs 2 and 3. "Intermediate" impact site tests consisted of striking the box section precisely over the taper-line which was one quarter of the distance from the right central web to the left central web, and is shown in the diagrams as impactor position (b). The taper-line is the drop-off of the ply and which is wrapped around from the web onto the skin, forming the taper. For the "web" impact site series of tests, the impactor struck the box section precisely over the right central web, and is shown as impactor position (c) in Figs 2 and 3.

3. Results

The continuous line plotted in the following graphs corresponds to a modified spring-mass model prediction of the elastic relationship between peak force versus total impact energy (TIE). The "term total impact energy" is described in an earlier work by these authors [4, 5] and equals $1/2\,mv_0^2 + mg\delta$, ($\delta =$ max. central deflection)

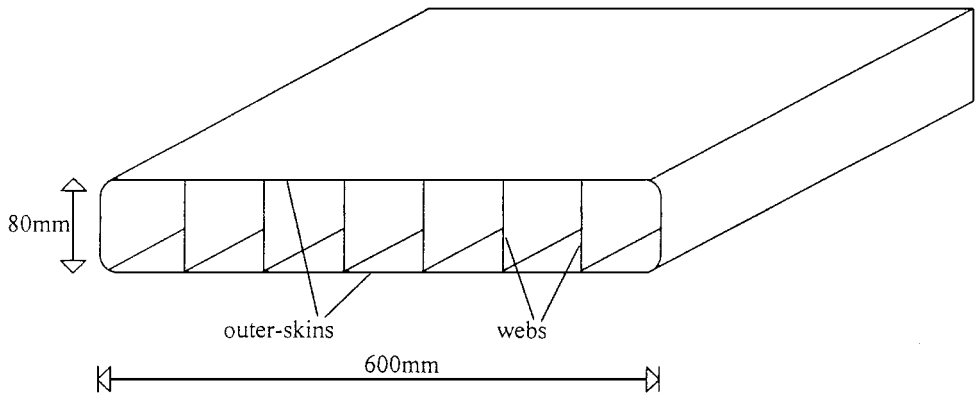

Figure 1 Simplified diagram of the pultruded section.

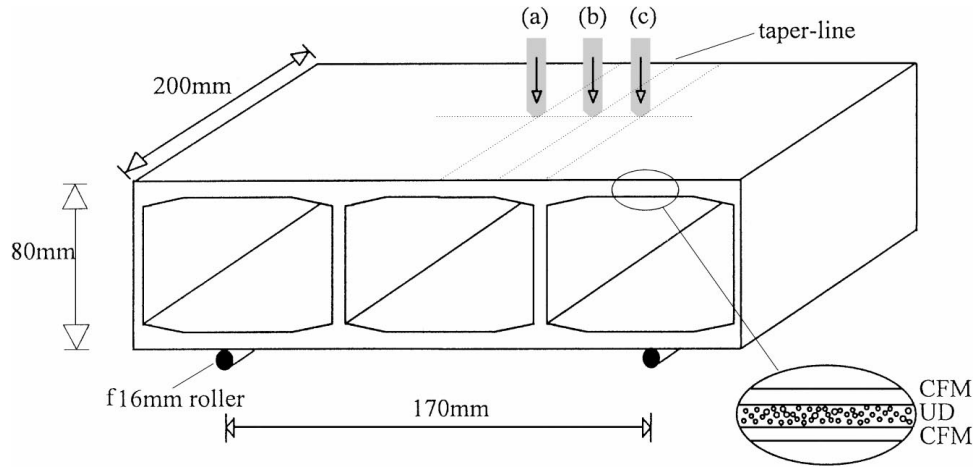

Figure 2 "Three-box section" impact test geometry and support conditions.

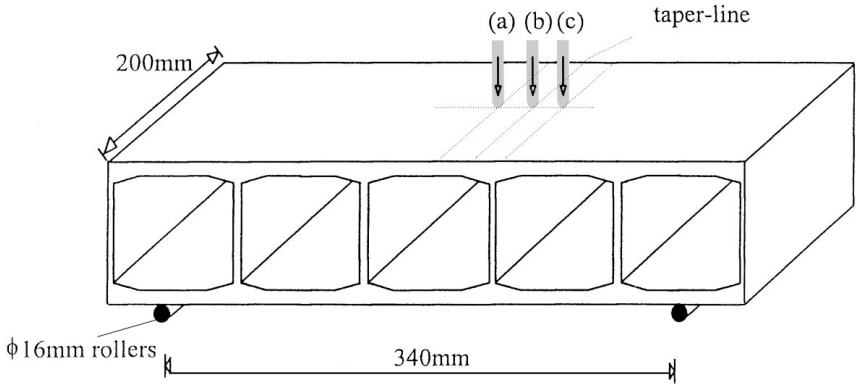

Figure 3 "Five-box section" impact test geometry and support conditions.

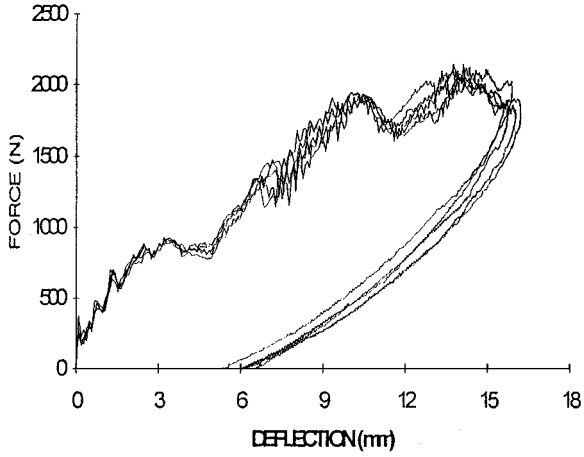

Figure 4 Force-deflection curve for the 21 J TIE central impacts from the three-box section.

which corresponds to the total energy absorbed by the specimen on a rebound test. The standard spring-mass model gives the following relationship between peak force and impact energy:

$$F_{\max} = \sqrt{(2U_0K)} \tag{1}$$

where $U_0 =$ impact energy (J), $K =$ initial stiffness measured from the force-deflection graphs (N/m). When this is inserted into Equation 1, it becomes

$$F_{\max} = \sqrt{(2 \cdot \mathrm{TIE} \cdot K)} \tag{2}$$

3.1. "Central" impact tests

Fig. 4 contains the force-deflection and force-time curves for all the impacts in the 21 J TIE set of three-box series of tests, showing a high vibration content but also a very repeatable response. Fig. 5 shows a steady rise in

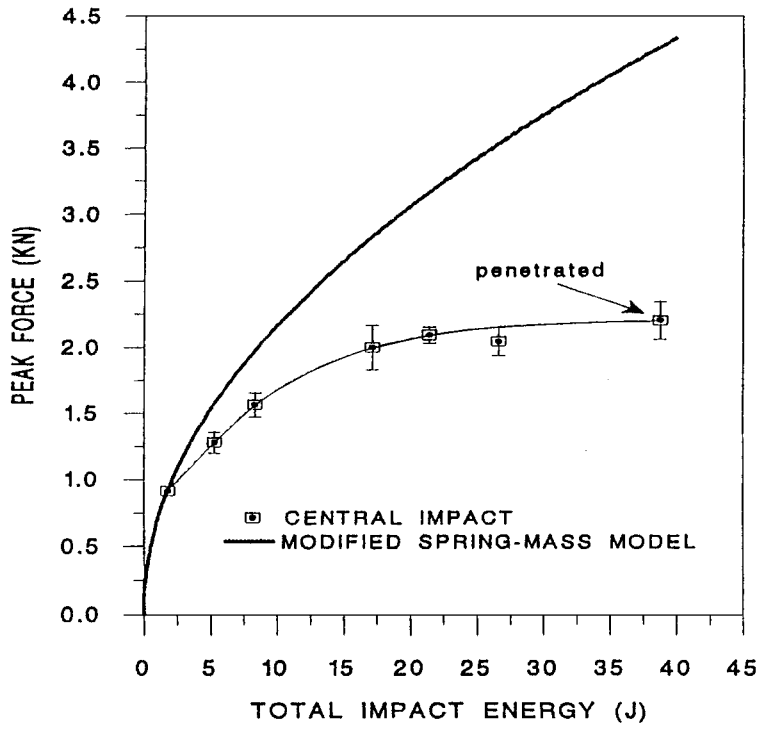

Figure 5 Peak force versus TIE for the central impacts from the three-box section and modified spring-mass model prediction.

peak force up to 8 J, a less steep rise between 8 J and 21 J and a flattening off thereafter, to the 38 J tests which penetrated the upper skin. With respect to the modified spring-mass model predictions, it is clear that only lowest energy impact approached an elastic response.

The first macroscopic damage was transverse cracking of the lower CFM layer, which was initiated above 2 J and grew with TIE to approximately 150 mm at which point penetration occurred. This crack initiated upper interface delamination as the crack propagated through the UD layer up to the upper interface (Fig. 6). Fig. 7a shows the close relationship between lower CFM crack length and upper interface delamination area and gives the CFM crack length required for upper interface delamination as 25 mm approximately. The relationship was less consistent at the highest energies due to both the penetration threshold being reached and the crack length approaching the width of the specimen.

Fig. 7b shows that upper interface delamination growth was relatively linear with TIE up to 21 J, at which point lower interface delamination was initiated which then increased linearly to penetration. The upper interface delamination, which was first detected at 5 J, was usually accompanied by a vertical (transverse) or inclined (shear) UD crack at or near its edge. (Fig. 6). The shear cracks in the UD layer, induced by the high shear forces generated by the double skin/web section, initiated lower interface delamination as shown in Fig. 8.

Fig. 9 shows a diagrammatic plan view of the typical upper and lower interface delamination shapes for a high energy impact, with the upper interface delamination following the CFM crack and the lower interface delamination forming outside the upper. The classic "peanut" shape was observed, with upper interface delamination suppressed directly under the impactor

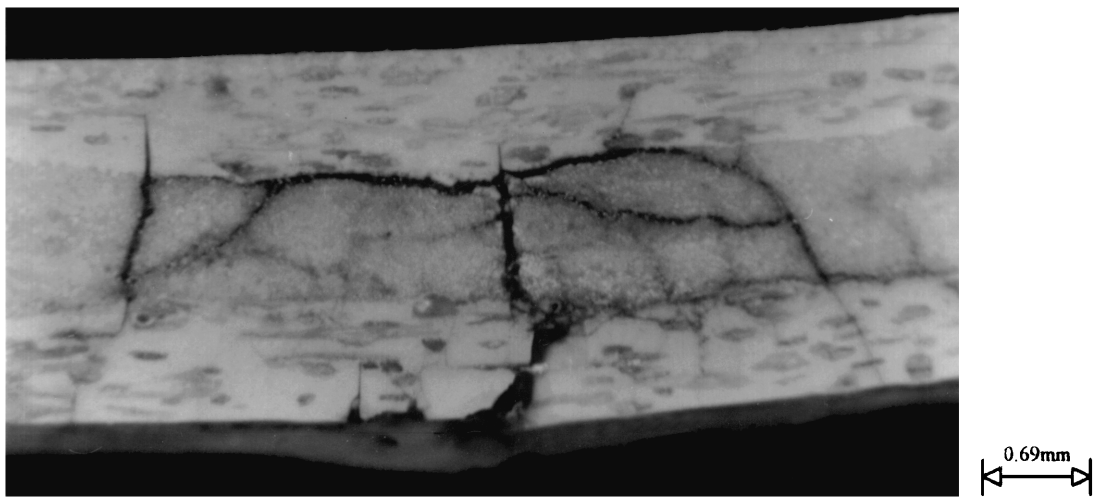

Figure 6 Photograph of UD cracking associated with upper interface delamination for 5 J TIE central impacts from the three-box section.

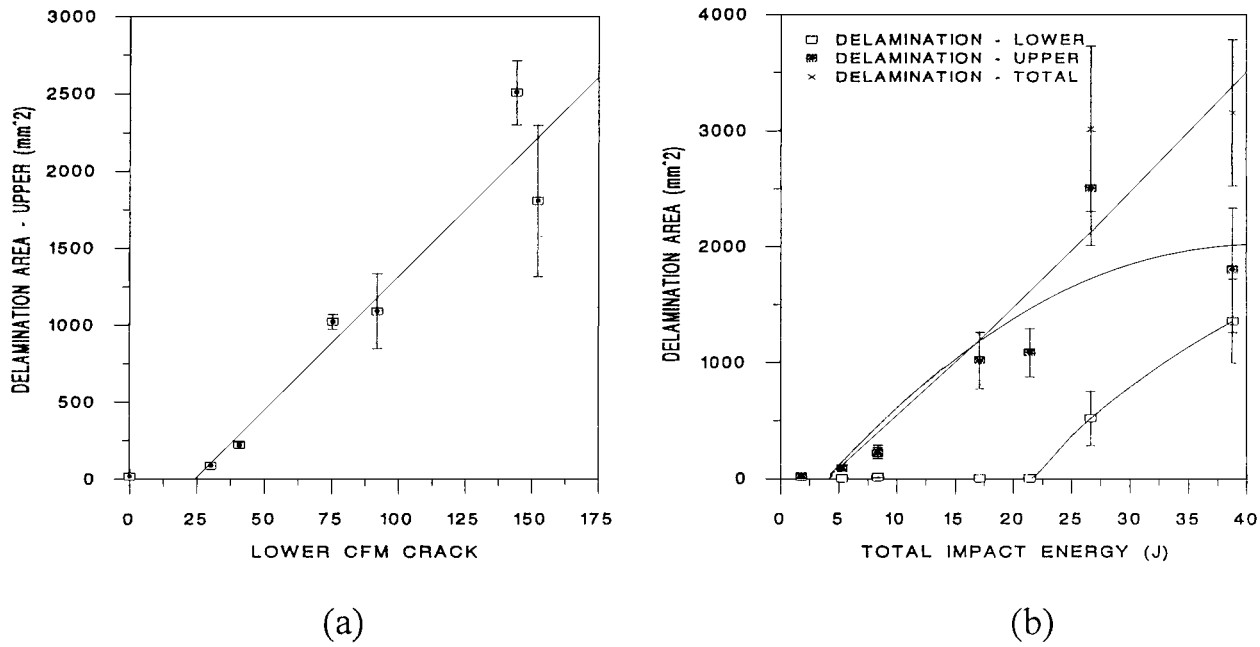

Figure 7 Upper interface delamination area versus lower CFM crack length (a) and delamination areas versus TIE for the central impacts from the three-box section.

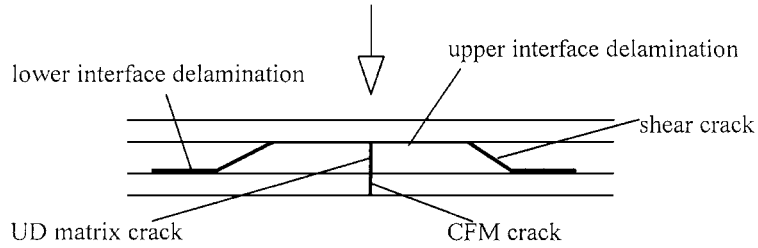

Figure 8 Shear cracking and delamination in central impacts from the three-box section.

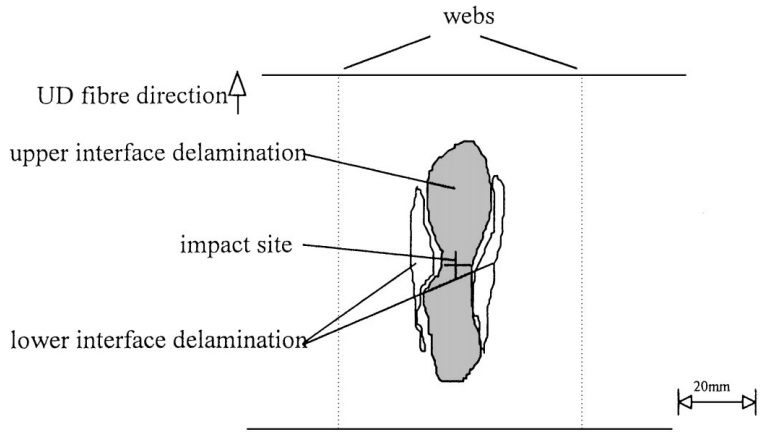

Figure 9 Upper and lower interface delamination shapes in central impacts from the three-box section.

due to the high compressive through-thickness stresses under the impactor.

Other forms of damage which occurred were shear cracking of the upper CFM layer and UD fibre breakage on penetration. The shear cracking was initiated in the 8 J set of tests and by 27 J the upper CFM layer was completely cracked through, therefore this form of damage also contributed to the lower peak forces above these energies.

The central impacts from the five-box section series of tests were very similar to the three-box section results described above, except that there was no lower interface delamination present. OM inspection revealed the absence of shear cracks in the UD layer from which lower interface delamination would be induced. This is due to the lower aspect ratio (span : depth) in the five-box section tests generating lower shear forces through the skin/web structure.

3.2. "Intermediate" impact tests

The force-deflection and force-time curves for the intermediate and web impacts were similar to those in Fig. 4 and so have not been repeated. The structural response and resulting damage progression of these specimens was more complex due to the non-symmetry of geometry and lay-up. In order to understand the results it is first necessary to study the exact lay-up at the web/skin join (Fig. 10). The fibres of the lower CFM ply and the wrap-around ply made of needle-mat do not intermesh, so the bond is dependent on the resin strength and was therefore an area of weakness.

Fig. 11a shows the peak force rising linearly to 9 J, flattening off thereafter at approximately 2.2 kN with penetration occurring for 38 J TIE tests. Only the lowest

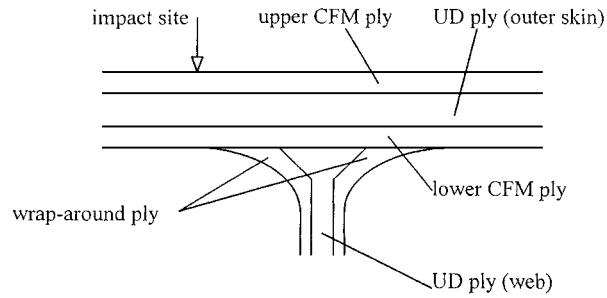

Figure 10 Typical transverse section through web-skin join.

energy response correlated well with the elastic response prediction.

The first form of visible damage was a longitudinal crack between the wrap-around ply and the lower CFM layer – a taper-line crack. The thermal deply (TD) exercise showed that there was no lower CFM crack at this point. The taper-line crack was not vertical and so did not directly initiate a matrix crack through the UD layer. Instead, it travelled between the CFM and needle-mat layers (Fig. 12) contributing towards the reduction in peak force from elastic predictions up to 9 J TIE. Fig. 11b shows that the taper-line crack grew linearly with TIE. This form of damage initiated a debond between the wrap-around ply and lower CFM layer, but even with optical microscopy it was not possible to identify the interface and so it was not possible to follow the crack growth. This form of damage will greatly reduce the compressive stiffness and strength of the section as stated by Davies and Robinson [7].

Optical microscopy revealed that both upper and lower interface delaminations were initiated above 2 J and both increased steadily up to penetration though the

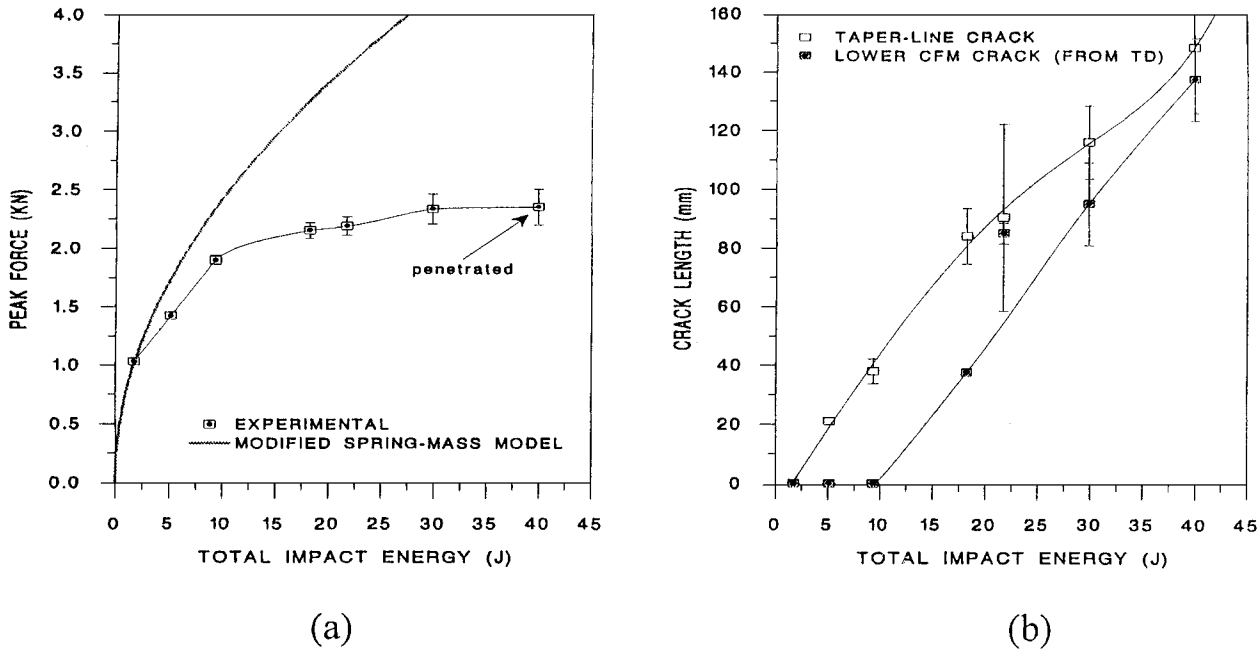

Figure 11 Peak force (a) and crack lengths versus TIE for the intermediate impacts from the three-box section.

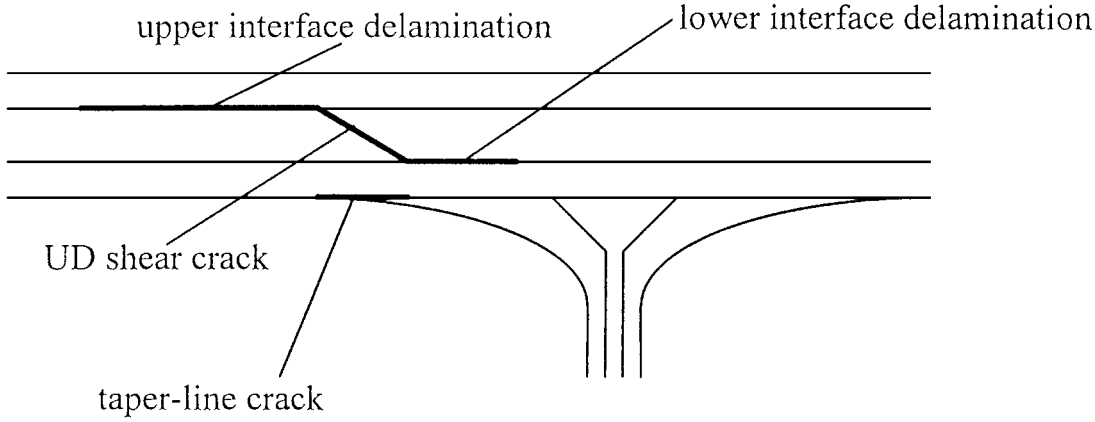

Figure 12 Damage progression in the intermediate impacts from the three-box section.

area of lower interface delamination was much lower than the upper (Fig. 13). The delaminations were initiated by a single shear crack in the UD layer under the impactor at approximately 45° pointing down towards the web (Fig. 14). The UD shear crack was present in the 2 J test specimens but with little or no associated delamination. Due to the non-symmetrical geometry and the much stiffer response on the web side of the impact site, high shear stresses were developed which initiated the shear crack and upper and lower interface delamination.

The upper interface delamination grew at a greater rate above 18 J (Fig. 13) whilst thermal deply showed that lower CFM cracking was first observed 9 J and 18 J (Fig. 11b). Due to the taper, the lower CFM crack could not be observed visually. The lower CFM crack, induced a UD matrix crack, which further promoted the propagation of the upper interface delamination. Lower CFM crack growth and greater rate of upper interface delamination correspond to the reduction in stiffness present in Fig. 11a between 9 J and 18 J TIE.

The initiation of lower CFM cracking was very dependent on the exact location of the impact. If the impact site was outside the wrap-around ply then lower CFM cracking occurred earlier, and behaviour tended towards that observed for the central impacts. When the impact site was over the warp-around ply, the damage forms discussed above postponed lower CFM cracking until later in the damage process.

A C-scan of a specimen from the highest energy set of tests is shown in Fig. 15, and Fig. 16 shows how the upper and lower interface delamination areas developed at higher energies. Clearly the damage was non-symmetrical along the impact site (i.e. the taper line), due to the non-symmetry of the geometry and therefore stiffness in the impact locality.

The non-symmetry of structural and damage response was also seen on the impacted surface. Little damage was induced on the CFM layer under the impactor on the side furthest from the web up to 22 J, but on the stiffer side nearest the web, shear cracking occurred and this side of the impact site collapsed at 18 J, which contributed to the flat curve above this TIE in Fig. 11a.

For the five-box section tests, the damage was generally of the same form as for the corresponding tests

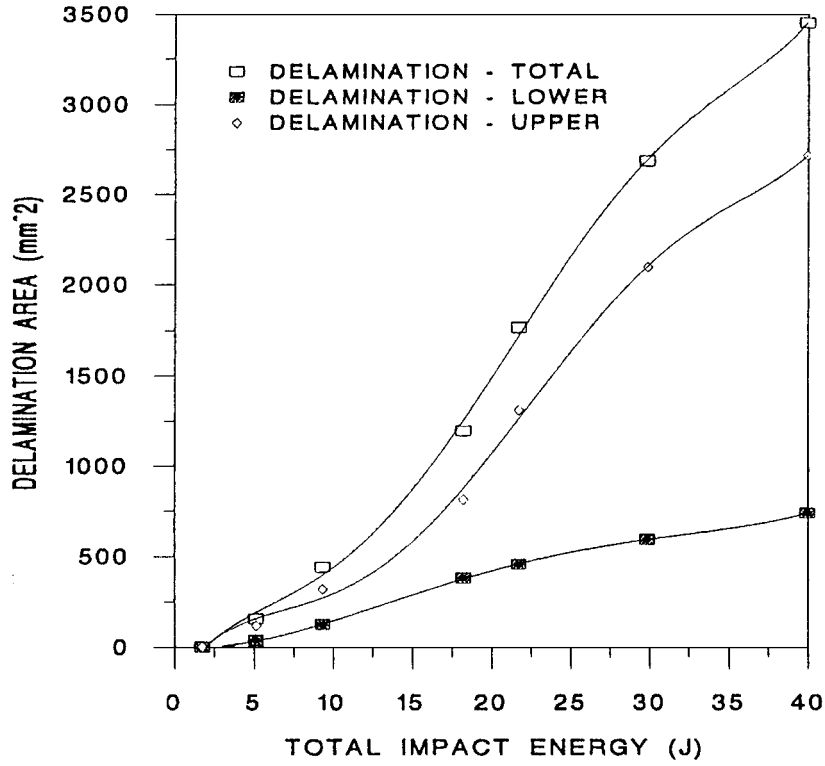

Figure 13 Delamination areas versus TIE for the intermediate impacts from the three-box section.

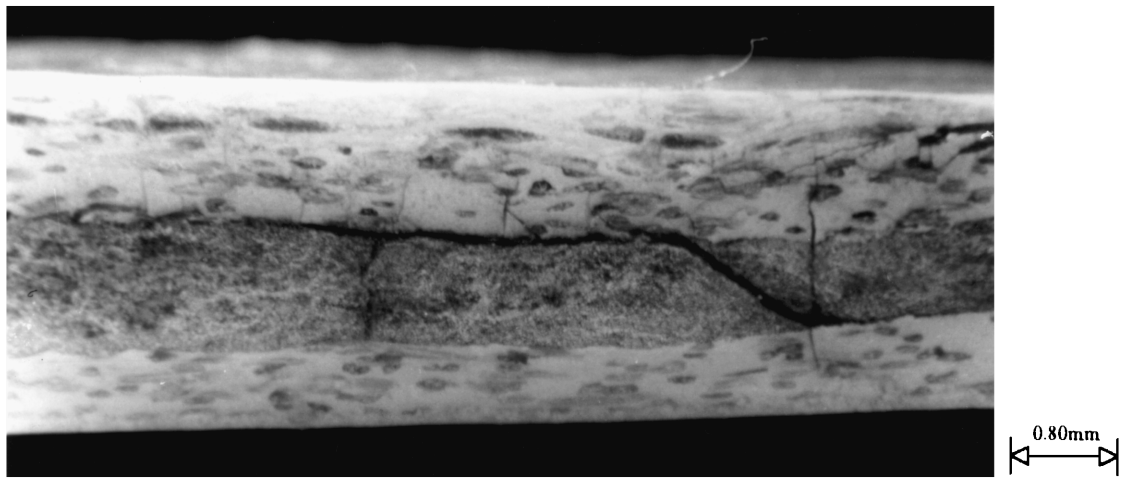

Figure 14 Photograph of upper interface delamination initiated by a UD shear crack for a 5 J TIE intermediate impact from the three-box section.

on the three-box sections. Shear cracking occurred first in the UD layer, which induced upper interface delamination and, at a higher energy, lower interface delamination. The lower interface delamination area was low due to the lower shear forces as explained previously.

3.3. "Web" impact tests

The impacts performed directly over the webs from the three-box sections elicited a completely different damage response from the central or intermediate impacts tests. Due to the nature of the damage the results have been treated descriptively rather than quantitatively. Fig. 17 contains the peak force versus TIE graph for all three test locations for the three-box section and clearly the forces generated in the web specimens were much greater than either the central or intermediate impacts indicating an entirely different response. The graph also shows that the peak force steadily departed from the elastic response curve, and flattened off above 40 J TIE ($\approx$ 5 kN).

For a strike directly over the web, due to the web itself, penetration cannot take place, whilst the impact damage was unpredictable because the response was critically dependent on the exact strike location, as there was a very large stiffness variation over a few mm's either side of the web.

In all the previous tests, local deformation under the impactor was superimposed on the global bending of the entire structure. For the strike location directly over the web, due to the high stiffness directly under the impactor very little local deformation occurred. Instead high stresses were transferred from the impact site on the upper skin throughout the structure via the webs.

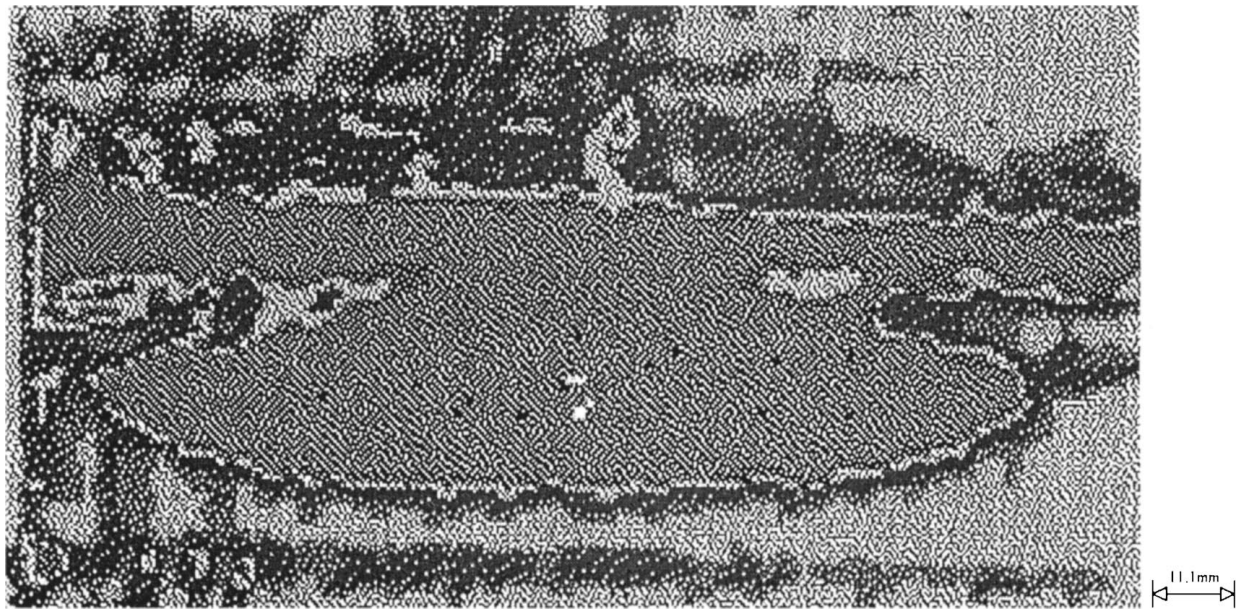

Figure 15 C-Scan of 40 J TIE showing damage area blending into the area indicating the web for an intermediate impact from the three-box section.

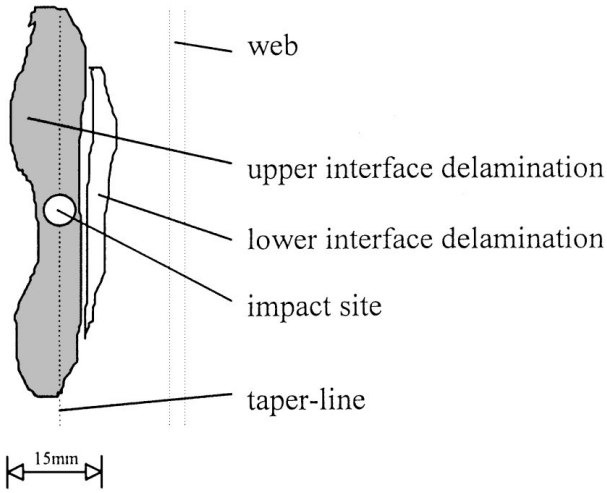

Figure 16 Delamination areas at high energy for intermediate impact from the three-box section.

Because there was little local deformation and therefore very low strains directly under the impactor, there was less local damage initially. The first damage, visible on the lowest energy tests, was a small permanent indentation under the impactor which arose due to the very high contact force.

The global deformation was responsible for absorbing the impact energy and therefore the damage, rather than originating and growing from under the impactor as previously, was initiated at remote sites as reported by Cheung [9]. The web/skin sections act as shear boxes and therefore the web/skin joins were particularly susceptible to damage. In addition to the geometry making these joins areas of stress concentration, the tight radii resulted in poor material and/or lay-up quality. Often resin rich or poorly wetted out fibres were found in these areas. Due to being both areas of high stress and often poor material quality, it was along these joins where the second form of visible damage occurred-matrix cracking (Fig. 18) and/or fibre whitening. At 50 J each section was permanently bowed due to the extent of this remote damage. Cheung and colleagues [9] identified the peeling stress on the skin/stiffener join due to bending as the reason for the remote delamination which they identified. In this work it was the tensile forces across the joins due to shear distortion of the boxes, which generated the cracking. The tensile forces caused matrix cracking whilst the compressive forces on the opposite join caused surface fibre buckling seen as fibre whitening.

On one of the specimens at 20 J TIE, there was a crack along the taper-line to the right of the impacted web due to a lay-up problem through the section at this point. One of the 70 J specimens for which the impact was directly over the web, had no local damage on the web/skin join under the impactor, but instead the web buckled along its length about halfway down its height. Both these examples illustrate how these impacts exploited local or remote weaknesses to a much greater degree than the others impact configurations.

For the five box-section series of tests no damage was visible local to the impact site except for a little local cracking at the skin/web join in a few of the specimens. No upper CFM shear cracking occurred due to the slightly lower contact forces than were present in the three-box section. The majority of the damage energy was therefore absorbed by cracking along the skin/web joins throughout the section, though there was no particular pattern to report, strengthening the argument that this form of damage was material/lay-up quality dominated. Due to the higher deflections recorded the cracking and creasing along the joins was more widespread than for the three-box sections. The peak forces generated in the shorter specimens (the three-box section) were, for each impact site, higher than for the longer specimens in the same location, due to the longer specimens being less stiff. The deflections at a given impact energy were therefore that much greater for the five-box section, which resulted in the impacts at all three locations causing more remote damage than for the three-box sections.

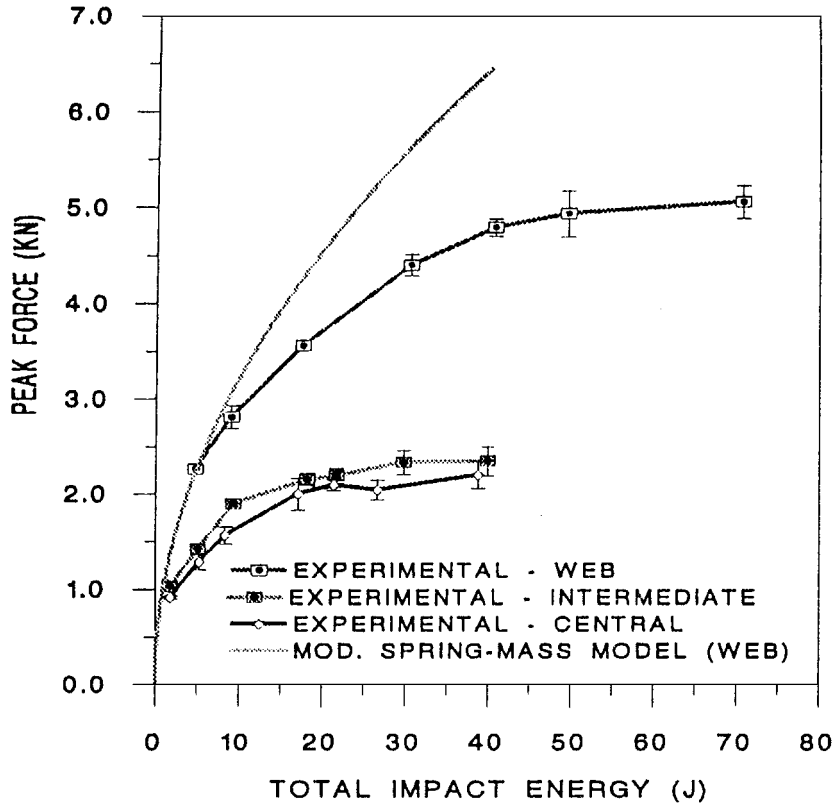

Figure 17 Peak force versus TIE for web, intermediate, and central impacts from three-box sections, and modified spring-mass model prediction for the web impacts.

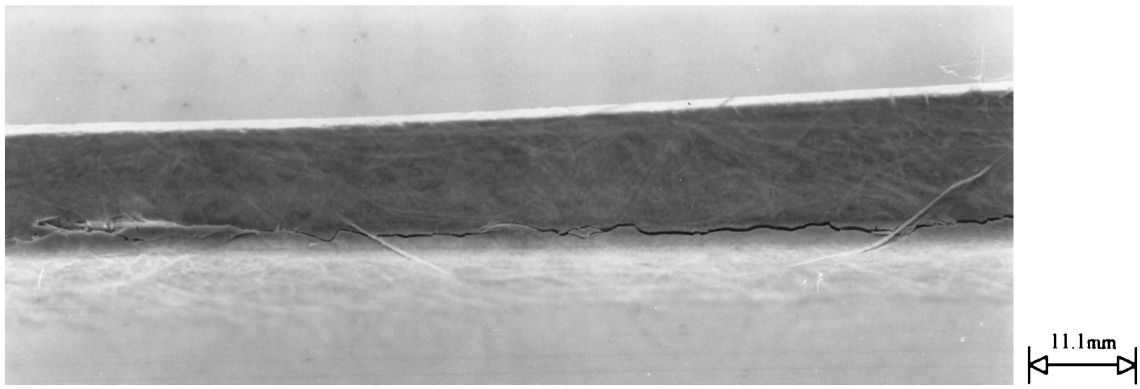

Figure 18 Photograph of matrix crack along skin/web join for a web impact from the three-box section.

4. Conclusions

- When impacted between the webs, the impact response could be defined by superimposing a local deflection directly under the impactor on top of a global deflection of the whole section. Due to the local deflection, damage was only initiated directly under the impactor. The central impacts from the three-box section exhibited damage which could be related to the response of the simple coupon tests[3], because there was no local complex geometry.
- An important transition in impact response was observed when the impact site was varied from between webs (simple geometry) to impacts over or near a web (complex geometry). As the impact site neared the web the response changed from local damage initiation, to a response dominated by remote damage at locations of stress concentration or poor material/lay-up quality. In the latter case the damage sites were unpredictable and far reaching, which has grave implications for residual strength of the whole structure and makes post-impact repair virtually impossible.
- The box sections introduced shear forces due to the double skin/webs design, with the span-to-depth ratio dictating the shear force levels, and therefore the modes of damage induced under impact loads.

Overall, this experimental impact test programme has provided a great deal of information regarding the impact response of the complex geometry structure of a typical double-skin/web pultrusion. The damage analyses have the danger of remote, extensive and unpredictable damage resulting from impacts in the vicinity of the webs.

Acknowledgements

We would like to thank our colleagues at Maunsell Structural Plastics, European Intermodal Products, Pera International and within Loughborough University for all their invaluable support during this research.

References

1. S. ABRATE, *Appl. Mech. Rev.* **44**(4) (1991) 155–190.
2. M. O. W. RICHARDSON and M. J. WISHEART, *Composites* **27** (1996) 1123–1131.
3. M. J. WISHEART and M. O. W. RICHARDSON, Low velocity response of simple geometry pultruded glass/polyester composite, submitted.
4. M. J. WISHEART, Impact properties and finite element analysis of a pultruded composite system, PhD thesis, Institute of Polymer Technology and Materials Engineering, Loughborough University, 1996.
5. M. J. WISHEART and M. O. W. RICHARDSON, Analysis of strain-rate effects on the low velocity impact response of a pultruded glass/polyester composite, submitted.
6. G. DOREY, Impact damage tolerance and assessment in advanced composite materials, Seminar on Advanced Composites – Cranfield Institute of Technology, 1986.
7. G. A. O. DAVIES and P. ROBINSON, Predicting failure by debonding/delamination, AGARD: 74th Structures and Materials Meeting, 1992.
8. G. A. O. DAVIES, X. ZHANG and A. EDLUND, Predicting damage in composite aircraft structures due to low velocity impact, Aerotech Conference, Birmingham, January 1994.
9. A. K. H. CHEUNG and M. L. SCOTT, Impact damage of thin skinned fibre composite panels, Australian Aeronautical 5th Conference, Melbourne, September 1993, pp. 155–160.
10. A. TABIEI, A. L. SVENSON and M. W. HARGRAVE, Impact behaviour of pultruded box-beams for roadside safety structures, 50th Annual Conference, Composites Institute, The Society of the Plastics Industry, January/February 1995, Session 10-D, pp. 1–6.
11. A. L. SVENSON, M. W. HARGRAVE, A. TABIEI, L. C. BANK and Y. TANG, Design of pultruded beams for optimisation of impact performance, 50th Annual Conference, Composites Institute, The Society of the Plastics Industry, January/February 1995, Session 10-E, pp. 1–7.
12. S. HONG and D. LIU, *Experimental Mechanics* **29** (1989) pp. 115–120.
13. N. D. PHAN and W. J. KESACK, Effects of damage on post-buckled skin-stiffener composite skin panels, American Helicopter Society, 45th Annual Forum, May 1989, Boston, pp. 1083–1090.

Received 1 March 1997
and accepted 18 August 1998